Supporting Information

for

A Force Field and a Surface Model Database for Silica to Simulate Interfacial Properties in Atomic Resolution

by

Fateme S. Emami[†], Valeria Puddu[‡], Rajiv J. Berry[§], Vikas Varshney[§], Siddharth V. Patwardhan[‖], Carole C. Perry[‡*], and Hendrik Heinz[†*]

†Department of Polymer Engineering, University of Akron, Akron, Ohio 44325-0301, USA

‡Interdisciplinary Biomedical Research Centre, School of Science and Technology, Nottingham Trent University, Clifton Lane, Nottingham NG11 8NS, UK

§Materials and Manufacturing Directorate, Air Force Research Laboratory, Wright-Patterson Air Force Base, Ohio 45433, USA

‖ Department of Chemical and Process Engineering, University of Strathclyde, 75 Montrose Street, Glasgow G1 1XJ, UK

* Corresponding authors: carole.perry@ntu.ac.uk, hendrik.heinz@uakron.edu

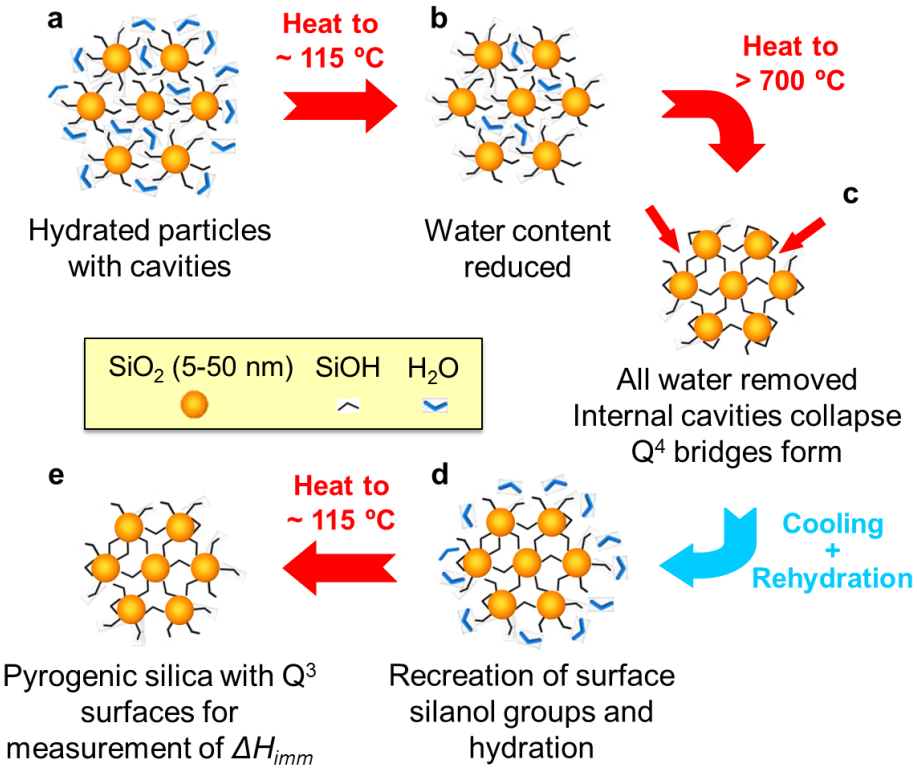

Figure S1. Preparation of pyrogenic silica particles with well-defined Q^3 surfaces with 4.7 silanol groups per nm^2 according to Taylor et al. in experiment (ref. [1]). (a) Silica particles are often agglomerates of smaller particles. The "superparticle" possesses intraparticle porosity, i.e., internal cavities. (b) Heat treatment at 115 ˚C removes surface water. (c) Further heating to 700 ˚C removes internal water, forming one covalently bonded "superparticle" without internal porosity. Also, Q^3 environments on the surface partially condense to Q^4 bridges. (d) Rehydration reconstitutes Q^3 environments. (e) Heating to 115 ˚C removes surface water and yields a uniform Q^3 like surface with defined area to measure the immersion enthalpy.

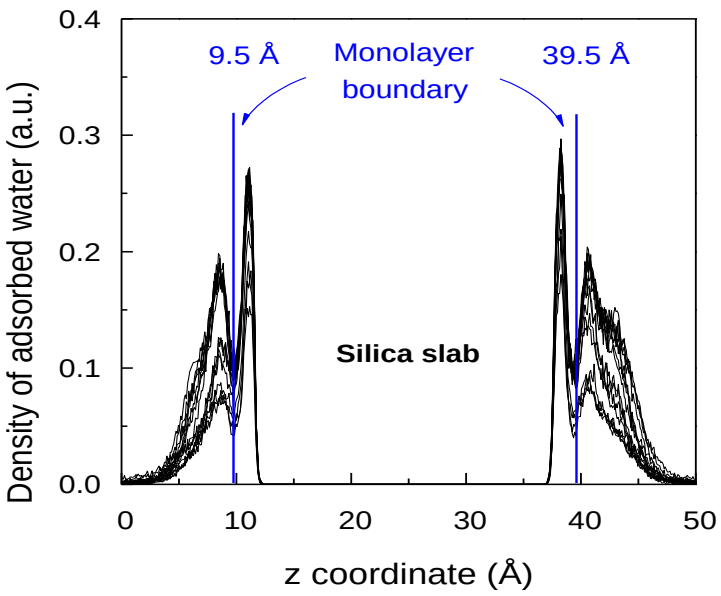

Figure S2. Density profile of water molecules adsorbed on the non-ionized Q^3 silica surface during to Gibbs ensemble simulations at 298.15 K. Nine plots for pressures of 0 to 1 kPa are superimposed and illustrate the formation of water agglomerates and multilayers even at a low fraction of monolayer coverage. The blue lines indicate the average z coordinate on both sides of the silica slab that separate adsorbed monolayers from higher order layers as an average over simulation time. The thickness of the monolayer was the same for all pressures.

Table S1. Density of α-quartz and α-cristobalite according to X-ray data and NPT molecular dynamics simulation under standard conditions for the different energy expressions. Uncertainties are given in brackets in units of the last digit. CVFF, CHARMM, and AMBER (equation 1) reproduce the density of α-cristobalite somewhat closer to experiment than PCFF (equation 2), and the same trend applies to the cell parameters (not shown).

Method	Density (g/cm^3)	
	α-quartz (5×5×5 cell)	α-cristobalite (6×6×4 cell)
X-ray	2.66 (4)[a]	2.32 (4)[b]
PCFF, CFF, COMPASS	2.68 (2)	2.43 (2)
CVFF	2.68 (2)	2.36 (2)
CHARMM	2.68 (2)	2.36 (2)
AMBER	2.64 (2)	2.32 (2)

[a] Ref. [2,3]. [b] Ref. [4].

Table S2. Heat of immersion of various types of silica particles.

Sample	ΔH (mJ/m^2)	Reference
Pyrogenic	160±5	[1]
Pyrogenic	164±10	[5]
Silica gel	190±10	[6]
Pyrogenic	201±20	[7]
Precipitated	365±10	[8]
Silica gel	392±10	[9]
Aerosil	505±15	[10]
Milled quartz	510±15	[10]
Milled quartz	880±10	[11]
Microporous & Miscellaneous	100-1300	Listed in [1]

S1. History of Force Fields for Silica

A number of interatomic potentials for silica have been developed to date (Table 1). Early force fields by Catlow,[12] Feuston et al.,[13,14] and Beest et al.[15] neglect covalent contributions to bonding and assume sharply overestimated atomic charges of +4.0e and +2.4e for Si. The simulation of Q^4, Q^3, and Q^2 surface environments with hydration and protonation equilibria is not feasible as covalent bonds play a dominant role and the excess ionic contributions prevent compatibility of the force fields with models of water and organic molecules, which require accurate polar and van-der-Waals interactions. Hill and Sauer[16,17] introduced covalent bonds and employed a more broadly applicable energy expression (CFF, PCFF).[16,18-20] Difficulties with the interpretation of atomic charges and van-der-Waals parameters were reported that lead to unstable, repulsive surfaces. An important conceptual advance was the consistent analysis of atomic charges for compounds across the periodic table and silica in particular in 2004,[21] as well as the atomic-level interpretation of LJ parameters in the context of measurements of surface properties.[22] The improved representation of chemistry and thermodynamic properties upgraded the accuracy of force fields for silicates, aluminates, phosphates, hydroxides, and metals up to two orders of magnitude[23-25] and has been applied to the silica model described here.

In the meantime, Cruz et al[26] developed a force field for amorphous silica consistent with the CHARMM energy expression and the TIP3P water model. Atomic charges and dispersive parameters of the atoms were considered variables to reproduce the contact angle of water on silica surfaces with different surface silanol density based on equation 3.[27] However, the interpretation of the parameters is not clear, fixed atoms are needed to avoid deformation, and the stoichiometry of the surface is not correct, including unsaturated valences of silicon and oxygen. Hassanali et al.[28] extended the van Beest and Kramer force field[15] to aqueous silica

interfaces using SPC/E rigid water molecules. Extra terms and adjustable parameters, called blocking terms, are used to avoid the formation of unphysical bonds at the interface. The extra terms add compatibility restraints to the less portable Buckingham potential and attempt to compensate the imbalance of ionic and covalent bonding. Chemical limitations remain because of the unchanged atomic charges (+2.4e for Si). Accordingly, the heat of immersion is 280 mJ/m^2 for surfaces with a silanol density of 4 nm^{-2}, corresponding to an overestimate of about 100% compared to experiment (the heat immersion increases with the area density of SiOH groups and experimentally amounts to 160 mJ/m^2 for 4.6 SiOH groups per nm^2). The value of 830 mJ/m^2 for 6.4 silanol groups per nm^2 is similarly higher than reported for quartz with Q^3/Q^2 environments (Table S2). Later extensions to include surface charge density do not correlate with experimental conditions.[29] Lopes et al[30] also introduced force field parameters for quartz surfaces compatible with the CHARMM force field. Tests of the force field against density and heat of immersion of quartz and cristobalite models showed that, if the structures were not fixed, more than 20% shrinkage occurs in comparison to the experimental density, and the heat of immersion was >1000 mJ/m^2 (>500% overestimate to experiment). The main reasons are unexplained high well depths ϵ_{ii} of 0.6 kcal/mol for silicon and 0.152 kcal/mol for oxygen. Therefore, the reported quantities of water interfaces such as layering effects, Vibrational Density of States (VDOS), Van Hove self-correlation function (VHSCF), and hydrogen bond formation are at most qualitatively justified. Moreover, Lockwood et al. introduced a multi-body potential for vitreous silica and protonated surfaces at low pH.[31] The atomic charges (+1.8e for Si) and melting temperatures (4000-6000 K) are overestimated so that interfacial simulations have significant limitations in accuracy.

Our team previously introduced a silica force field consistent with PCFF that is similar to the current model, overcomes many prior limitations, and included surface ionization for the first time.[25] Subsequently, Butenuth et al.[32] presented a silica force field that also considers deprotonation of surfaces and hydration energies. The parameters are fitted using *ab* initio calculations without interpretation. When the model was tested for reproduction of the cell parameters, >30% compression occurred that could be related to overestimated atomic charges (+1.6e for Si and -0.8e for O). An alternative to simulate reactive transformations of silica could also be ReaxFF.[33] However, surface properties are not well reproduced and the complex energy expression has no compatibility for interfaces with water, polymers, and biomolecules in its present form.

The aim of this contribution is the introduction of a silica force field that represents a complete solution for the above challenges, based on earlier accurate force fields for layered silicates, aluminates, ring silicates, and inosilicates.[22,24,25,34,35] The force field is fully consistent with what is known of the chemical properties of silica at the atomic and interfacial scale.[1,3,4,27,36-50] The parameters originate from the 2012 silica force field,[25] include refinements of Lennard-Jones parameters, and additional full coverage of the CHARMM, CVFF, and AMBER force fields. The parameters have also become part of the INTERFACE force field[24] and a comprehensive surface model database is introduced that provides realistic surface models for any silica surface chemistry and pH, encompassing the range of Q^2, Q^3, and Q^4 environments for variable ionization. The silica force field allows unrestricted atom mobility and reproduces dipole moments, X-ray structures, density, IR spectrum, hydration energies, contact angles of water, adsorption isotherms of water, zeta potentials, and adsorption free energies of peptides in quantitative agreement with experimental measurements (see ref. [51] for data on peptides). In

particular, the feasibility to analyze a wide range of properties of aqueous interfaces, adsorption isotherms, and electric double layers contributes much needed atomic-level understanding. Perhaps the most important advance is the feasibility of quantitative estimates of the binding of biomacromolecules as a function of pH and surface type (particle size) in agreement with measured adsorption isotherms.

S2. Further Information on Silica Surface Models

Common amorphous silica nanoparticles such as those prepared by a Stöber-like synthesis are neutral at the point of zero charge (pzc) between pH 2 and 4 (Figure 2).[25] At higher pH, silanol groups on the surface (Si-OH) dissociate and form alkali siloxide groups. Surface ionization increases with higher pH, larger particle size, and also higher ionic strength of the solution.[25,36,39,41,43,45] At pH ~7 and an ionic strength similar to physiological conditions (0.1-0.3 $mol \cdot dm^{-3}$), deprotonation of silanol groups amounts to between 5% and 20% on Q^3 like surfaces with a total average area density of Si-O(H,Na) groups of 4.7 per nm^2, corresponding to between 0.25 and 1.0 siloxide groups per nm^2 (Figure 2).[36,39,41,43,45] Crystalline silica tends to display a higher charge density in comparison to amorphous silica and may exceed 25% ionization at pH 8. Silica dissolution by alkaline hydrolysis begins at pH >9. The properties of aqueous interfaces are specifically analyzed in section 4 in the main text.

The models illustrated in Figure 1 represent crystalline and amorphous silica surfaces of different topology at various pH values. Q^3 surfaces are common for amorphous silica and porous glasses (Figure 1a-c).[49] Q^3 surface models were derived from the $(10\bar{1})$ cleavage plane of α-cristobalite to provide reproducible structures and energies, which can be a challenge for amorphous models (Figure 1d).[4] 0% ionization corresponds to silica at the point of zero charge,

ca. pH~2-4 depending on particle size (Figure 1a), ~9% ionization corresponds to pH~5-7 (Figure 1b), and ~18% ionization corresponds to pH~7-9 (Figure 1c). Our assumption of the degree of ionization is approximate physiological conditions, i.e., 0.1-0.3 $mol \cdot dm^{-3}$ sodium chloride. Customization of models for other conditions is possible (see also surface model database in the SI).[19,36,41,43-45]

Models of other common topologies include amorphous surfaces, Q^2 containing surfaces, and Q^4 containing surfaces (Figure 1d-f). Amorphous surfaces can be insightful in comparison to surfaces with a regular repeat although arbitrary internal configurations and reduced structural stability can become a challenge for reproducible simulations (Figure 1d). The total area density of silanol and siloxide groups on amorphous models is shown equal that on Q^3 surfaces as 4.7 nm^{-2} and the degree of ionization as ~3.8 Si-OH and ~0.9 $SiO^{-}\cdots Na^{+}$ groups per nm^2 (18%) similar to that expected at pH values between 7 and 9. Mixed Q^2/Q^3 surfaces and Q^2 surfaces can be found on large nanoparticles (>200 nm) and on certain facets of quartz (Figure 1e). The model of a pure Q^2 surface was derived from the (100) cleavage plane of α-quartz and contains 9.4 Si-O(H, Na) groups per nm^2. The dominance of geminal and vicinal silanol groups increases the acidity of this surface relative to Q^3 surfaces. The visualization shows ionization at the very upper limit with ~7.5 Si-OH and ~1.9 $SiO^{-}\cdots Na^{+}$ groups per nm^2 (pH~9 at high ionic strength). Q^4 containing surfaces result from pretreatment of silica at temperatures between 500 and 1300 K. These conditions lead to condensation of hydrophilic silanol groups to siloxane bridges and yield less hydrophilic surfaces (Figure 1f).[1,49] The model shown contains a total of ~2.4 Si-O(H, Na) groups per nm^2 and 100% hydroxylation, corresponding to the pzc.

Energy minimization of various structures of ionized surfaces with different possible distributions of siloxide groups for a given degree of ionization showed that an approximately

even distribution of ionic groups is preferred to minimize Coulomb repulsion. The inclusion of proton mobility in the simulation would not significantly change this tendency, although surface-adsorbate interactions might slightly increase.

The models can be extended to porous morphologies, zeolite structures, as well as metal organic frameworks (the latter may require extensions of force field parameters).

S3. Derivation and Interpretation of Force Field Parameters

S3.1. Overview, X-ray Structure, and Atom Types. The protocol for the derivation of parameters involves (1) the retrieval of suitable X-Ray structures, (2) the definition of atom types, (3) the derivation of atomic charges, (4) initial assignment of Lennard-Jones and bonded parameters, (5) computational test of density and geometry including parameter refinements, (6) computational tests of surface properties including parameter refinements, (7) secondary validation and refinements of further bulk and surface properties, leading to the final model.[24]

X-Ray structures of α-quartz and α-cristobalite were chosen to parameterize the model since they are stable under reference conditions of 298 K and 101.3 kPa and within a considerable range of temperatures and pressures nearby.[2-4] Five chemically distinct atom types were defined to enable accurate computations of structural and surface properties in high quality, and to keep the number of atom types to a minimum. The five atom types include (1) silicon atoms that may carry a default charge of +1.1e or a charge of +0.725e if a siloxide group is attached, (2) bulk oxygen atoms with an atomic charge of -0.55e, (3) surface silanol oxygen atoms that carry a charge of -0.675e in silanol groups or -0.9e in siloxide groups, (4) silanol hydrogen atoms with a charge of +0.40e, and (5) sodium ions that carry a charge of +1.0e (Figure 3).

S3.2. Atomic Charges. The atomic charges q_i represent covalent and ionic contributions to chemical bonding in silica and require high chemical accuracy to achieve internal consistency of the force field as well as compatibility of the silica force field with parameters for other compounds such as water, organic compounds, ions, and other minerals (Figure 3). We explained these aspects in 2003[52] and analyzed atomic charges for silica, alumina, and clay substitution sites in high accuracy.[21] The atomic charge of silicon in tetrahedral oxygen coordination was shown to be +1.1±0.1e in agreement with electron deformation densities, dipole moments, an extended Born Model, comparisons to related compounds across the periodic table, and observed reactivity of Si-O bonds in chemical reactions.[21] The corresponding charge on oxygen atoms in bulk silica is -0.55e.

Oxygen atoms in silanol groups experience an increased charge (-0.675e) due to the presence of acidic hydrogen atoms (+0.40e) that attract more positive charge per O-H bond than silicon atoms per Si-O bond (+0.275e). Atomic charges for silanol hydrogen at the surface were initially estimated similar to water as +0.4e on the basis of the known significant acidity (pK 6-8). Tests to verify this initial assumption involved the computation of the immersion energy of Q^3 surfaces in water in comparison to measurements, including variations of the silanol hydrogen charge and the Lennard-Jones (LJ) parameters of silanol oxygen. The charge of -0.675e of silanol oxygen followed from charge neutrality. It offsets the sum of contributions from silicon (1/4 of +1.1e) and hydrogen (+0.4e). The charge of -0.675e for silanol oxygen atoms is also in the range of values -0.6e to -0.7e that maximize the electron affinity of oxygen.

In siloxide groups, silicon atoms receive a lower positive charge (+0.725e) and oxygen atoms a higher negative charge (-0.9e) due to the exchange of hydrogen (+0.40e) for sodium ions (+1.0e). The corresponding negative charge (-1.0e) from Na^+ ions is spread predominantly on the

monovalent siloxide oxygen (-0.275e + (-0.625e) = -0.9e) and partly on the siloxide silicon atom (+1.1e -0.375e = +0.725e) according to electronegativity differences.[21] The hypothetical maximum total negative charge on siloxide oxygen according to electroneutrality (-1.275e with contributions of -1.0e from sodium and -0.275e from Si) thus partially neutralizes the positive charge of +1.1e on silicon to +0.725e. The resulting O charge in siloxide upon formation from silanol is -0.90e with an uncertainty of ±0.1e. Additional support comes from similarities to oxygen charges of -0.925e and -1.0e in siloxide groups of tobermorite 11 Å and 14 Å, which are similar to aqueous silica and reproduce cell parameters and surface tensions in agreement with measurements.[24] The siloxide oxygen charge is also similar to -1.0e in Ca_3SiO_5, which is slightly more ionic due to the presence of Ca^{2+} ions and has also demonstrated accurate cell parameters and cleavage energies.[35]

A clear interpretation of atomic charges q_i and the validation of van-der-Waals parameters (Lennard-Jones parameters $\sigma_{0,ii}$ and $\varepsilon_{0,ii}$) in comparison to experimentally measured surface and interface properties is vital for a reliable force field (Figure 3 and Table 3). Similar atomic charges q_i were also identified in layered silicates and in calcium silicates to reproduce electrostatic contributions to surface tensions and cleavage energies.[22,24,34,35] In addition, surface properties of several chain and ring silicates containing SiOH and SiO^- groups are also reproduced in excellent agreement with experiment using these charges.[24] Electrostatic contributions to surface properties scale with the square of atomic charges q_i^2 and are thus sensitive to accurate values.

S3.3. Bonded and Lennard-Jones Parameters. The initial assignment of bonded parameters relies on the X-ray structure and IR/Raman spectra (Table 4). The parameter $r_{0,ij}$ for the equilibrium bond length of Si-O bonds follows from the average bond length of 1.61 Å

according to X-ray analysis with a small increase of +4% (CHARMM, CVFF, PCFF, COMPASS) and +2.5% (AMBER) as 1.68 Å and 1.65 Å, respectively.[2-4] The increase offsets superimposed contraction by Coulomb nonbond forces, especially between 1,4 bonded atoms, and ensures that equilibrium bond lengths of 1.61 Å are reproduced in NPT simulation at 298 K and 101.3 kPa. Specific differences in the increase of $r_{0,ij}$ relative to the X-ray equilibrium bond length are associated with the scaling of nonbond interactions between 1,4 bonded atoms. Full inclusion of attractive nonbond interactions between 1,4 bonded atoms in most force fields (CHARMM, CVFF, PCFF, COMPASS) requires a 4% increase in $r_{0,ij}$. Partial inclusion of attractive nonbond interactions between 1,4 bonded atoms (50% of Lennard-Jones interactions and 5/6 of Coulomb interactions in AMBER) requires only a 2.5% increase, and 12-6 LJ parameters identical to these in CVFF and CHARMM can then be used. The O-H bond length was chosen according to known data from silicic acids and water molecules.[53] The parameters $q_{0,ijk}$ for bond angles follow from X-ray structures and were slightly modified to reproduce equilibrium bond angles in NPT simulation under standard conditions. The vibration constants k_r and k_q of Si-O bonds, O-H bonds, and angles were initially chosen according to tabulated force constants[53] and force fields for similar silicates.[22,35] IR and Raman spectra were then computed from short MD trajectories with the initial parameters (section S9.3) and compared to experimental data, followed by refinements of the force constants k_r and k_q for best agreement.[22]

Van-der-Waals parameters σ_{ii} and ε_{ii} were assigned on the basis of known atomic radii,[54] polarizability,[55] and the numbers of nonbonded neighbors in the nearest coordination shells

(Table 3).[24] Accordingly, values of ε_{ii} of bulk and silanol oxygen atoms are distinguished, while oxygen atoms in Si-OH and Si-O^- groups can be treated the same.

S3.4. Computational Test of Density and Geometry. The initial set of parameters was used to compute the cell parameters of α-quartz and α-cristobalite in NPT simulation. Bond lengths $r_{0,ij}$ and angles $\theta_{0,ijk}$ as well as Lennard Jones parameters σ_{ii} and ε_{ii} were then fine-tuned to minimize deviations in a series of iterative calculations with systematic variation in a reasonable range. The initial fit before refinement lead to less than 5% deviation from experiment.

S3.5. Computational Test of Surface Properties. The parameters with the highest initial uncertainty are the well depths ε_{ii} because the value depends on the volume density of nonbonded neighbors for chemically similar atoms as a consequence of pairwise summation. In a framework of covalent bonds such as bulk silica, for example, the number of nonbonded oxygen neighbors per unit volume is higher and a lower ε_{ii} value needs to be chosen. In a largely nonbonded environment such as water or on a silica surface, the number of nonbonded oxygen neighbors per unit volume is lower and a higher ε_{ii} value needs to be chosen (Table 3). An accurate final assignment of ε_{ii} is possible on the basis of known interfacial properties, e.g., surface tension, interface tension, cleavage energy, heat of immersion in solvents, adsorption isotherms, contact angles, and zeta potentials.[22,24] Usually agreement of just one of these properties in computation and experiment leads to good reproduction of the others so that a choice of one property for initial validation can be made on the basis of availability and accuracy of experimental measurements. For a material such as silica with many possible surface morphologies and surface reactivity, the selection of reproducible experimental data is challenging. For example, cleavage energies are not suited for force field validation due to dissociation of covalent bonds, and surface tensions or interface tensions are ambiguous due to

surface reconstruction, surface reactivity (hydration, ionization), as well as additional assumptions in the calculation from surface pressure measurements.[56] On the other hand, the heat of immersion is accessible through calorimetric measurements[1,5] and was applied to validate properties of Q^3 silica surfaces with negligible (<1%) degree of ionization (see sections 4.1 and S5 for details). To achieve accurate reproduction of the heat of immersion in water of 160±5 mJ/m^2, the Lennard-Jones well depths ϵ_{ii} for silanol oxygen were systematically varied, along with minor variations in H and silanol oxygen charges for additional testing (no final adjustments in charges were required).

S3.6. Secondary Validation and Refinements. Further validation of the parameters included computed contact angles of water on various silica surfaces with Q^3, Q^3/Q^4, and Q^4 termination in comparison to measurements, computed adsorption isotherms of water in comparison to experimental data, and the amount of dissociated cations on ionized Q^3 surfaces in comparison to experimental zeta potential measurements. The agreement was quantitative or qualitatively very good without further parameter adjustments, as similarly observed for thermodynamically consistent parameterizations of other compounds upon initial parameterization.[22-24,35] The calculations also provide significant new insight into the molecular structure of these interfaces (see sections 4 and S7).

Limitations remain in the reproducibility of mechanical properties. Computed bulk moduli are up to 100% overestimated, related to the superposition of bonded terms for the continuous covalent framework with attractive Coulomb interactions and repulsive Lennard-Jones interactions. Similar observations were made for the in-plane Young's modulus of layered silicates[57] while minerals with a discontinuous network of covalent bonds, such as tricalcium

silicate, tobermorites, and hydroxyapatite, exhibit near perfect agreement of computed bulk and Young's moduli with experimental data (<10% deviation).[24] Details follow in section S4.

The force field was then transcribed from the energy expressions with 9-6 Lennard-Jones parameters (equation 2) to the energy expressions with 12-6 Lennard-Jones parameters (equation 1). This procedure involved adjustments of the LJ parameters σ_{ii} and ε_{ii} in 9-6 to the 12-6 form following previously described relationships, followed by renewed validation and refinements in the 12-6 form.[22-24,35] The final force field was tested again for densities, surface properties, and vibration spectra in all energy expressions (PCFF, CVFF, CHARMM, AMBER) and found to yield essentially identical results (Table 5 and Table S1).

S3.7. Summary. It has been demonstrated for silica, as part of a range of other compounds,[21,22,24] that validation of interfacial properties enables agreement between simulation and experiment with ±5% deviation (better than ±10% in high confidence), in contrast to deviations up to several 100% with earlier models. Due to the interpretation of force field parameters in the context of atomic-scale and macroscopic data, the force field provides insight in atomic resolution that remains unavailable by imaging techniques. Such properties include, for example, interface tensions, cleavage energies, heats of immersion, adsorption isotherms, contact angles, and zeta potentials. The limited number of final force field parameters also represents a simplified "code" to describe such complex properties.

In total, more than 1000 simulations were performed to validate the force field and systematically understand the influence of individual parameters. The detailed analysis of adsorption of peptides as a function of pH and particle size expounds the predictive abilities further (described in a separate manuscript, ref. [51]).

S4. Mechanical Properties in Experiment and Simulation

S4.1. Elastic Moduli. Bulk moduli for α-quartz are 35-45 GPa according to X-Ray measurements and Brillouin spectroscopy, of which 36 GPa is often reported.[58-60] Bulk moduli for α-cristobalite are 11-17 GPa in experiment and 11.5 GPa is most often reported.[4,7,58] Computed bulk moduli are 72±6 GPa for α-quartz and 36±3 GPa for α-cristobalite using either PCFF, CHARMM, or AMBER. It is understood that the superposition of the dense network of covalent bonds with the added presence of Coulomb and Lennard-Jones interactions cause the overestimated computed values, similar to the in-plane Young's modulus of layered silicates.[57] The bonded parameters are fitted to vibration constants from IR and Raman spectra, which possibly could alone reproduce the elastic properties; added attractive-repulsive contributions from nonbond interactions likely augment the elastic moduli. In essence, covalent contributions to bonding are overvalued by assuming full covalent bond strength, which ought to be only a fraction of the total with the appropriate measure of ionic contributions accounting for the rest, thus leading to excessive stiffness. In agreement with this argument, the INTERFACE parameterization reproduces elastic constants with less than 10% deviation from measurement for other partly covalent compounds that exhibit some nonbond-only interactions between individual bonded building blocks, e.g., tricalcium silicate, tricalcium aluminate, and hydroxyapatite. While a similarly accurate solution for silica requires further work, the current silica force field still achieves a substantial improvement in computed mechanical properties over prior silica force fields embedded in biomolecular force fields, since these models provided no structural stability and thus elastic moduli were either negative or excessively large.

S4.2. Opportunities by Nonbonded Silica Force Fields such as Van Beest, Kramer, and van Santen (BKS). Elastic properties and phase conversions of different silica polymorphs can

be reproduced using nonbonded-only potentials such as the force field for crystalline silica by Van Beest, Kramer, and van Santen (BKS).[15] The BKS potential offers the advantage to study different polymorphs of silica such as quartz, cristobalite, coesite, stishovite, molecular sieve silicates, and other silicate phases. The accuracy of structural and mechanical properties is good over a range of temperature up several thousand °C and pressures so that different phases of silicon dioxide and phase transitions in silicate glasses at high temperatures can be analyzed. On the other hand, the neglect of covalent bonding contributions and compensation by a high atomic charge of +2.4e for Si introduce deviations in polarity and surface properties by several 100%, not allowing meaningful simulations of interfaces with solvents and soft matter (Table 1).

S4.3. Advantages and Disadvantages of the BKS Potential. The BKS parameters for crystalline silica[15] consider exclusively non-bonded interactions, including an attractive Coulomb potential as well as a Buckingham potential for dispersive and repulsive van-der-Waals interactions. The parameters were obtained by ab-initio calculations on small silica clusters. Interpretations of the parameters are missing and empirical adjustments were made to reproduce silica bulk properties such as elastic modulus and cell parameters.

As we have shown, covalent bonding contributions dominate over ionic bonding in silicates in an approximate ratio of 75% versus 25%.[21] In the BKS model, this balance is skewed towards ionic bonding and incoherent electrostatics becomes the leading cause of limitations. The lack of cohesion from covalent contributions is compensated by overestimated atomic charges q (+2.4e on Si instead of +1.1e) that correspond to 218% of the true value according to measurements and theory.[21] Coulomb cohesion scales with q^2 and then amounts to about 4.7 times the true value, approximating the cohesion of the real system without covalent bonds (100% ionic instead of 75% covalent/25% ionic). Therefore, mechanical and structural properties do correlate well with

experimental data. The artificial polarity and associated excessive dipole/multipole moments, however, do not permit consistency with aqueous and organic interfaces even if bond and angle parameters for chemically different surface groups such as SiOH or SiO^- Na^+ would be added. The result, if computed, are surface and hydration energies that overestimate measurements by multiples.[28,29] In addition, the Buckingham potential remains difficult to integrate in common harmonic force fields.

This example shows that chemically consistent parameterizations can explain strengths and weaknesses of alternative models and how they might be improved.

S5. Details on Heat of Immersion

The variability of the structure and surface chemistry of silica depending on synthesis protocol, pretreatment, and aqueous conditions (pH, ionic strength) results in a large spread in reported heats of immersion between 100 and 1300 mJ/m^2 (Table S2).[1,5-11] Nevertheless, specific values for each silica sample can be rationalized by consideration of silica morphology and surface chemistry (Figure S1).

Hydration energies at the high end were reported for silica gels that contain a large fraction of nanometer-size pores. The pores contain additional interfacial area for hydration and induce capillary effects. Similar observations were made for precipitated particles with high porosity and internal cavities (Figure S1a). A large heat of immersion of >500 mJ/m^2 is also reported for quartz particles without pores, which stems from the Q^2 topography of quartz surfaces with higher area density of silanol groups compared to the usual Q^3-like topography of amorphous silica (Figure 1e versus Figure 1a-d).[10] Some non-treated quartz particles may feature particularly reactive and non-relaxed functional groups at the interface resulting from crushing

procedures of large crystals into fine particles in large-scale production facilities.[61] The measured specific area in these cases often refers to a near-spherical agglomerate particle (Figure S1a) while hydration proceeds on all intra-agglomerate pores and Q^2 features, increasing the hydration energy per surface area up to multiples. At the same time, initial hydration of the particle surface due to humidity and occluded water can also diminish the remaining energy of hydration.

Kiselev has shown that the most appropriate type of silica particles for physicochemical quantity measurements may be pyrogenic silica particles (Figure S1) or amorphous silica particles with uniformly wide pores.[50,62] Careful surface characterization and well-defined sample preparation procedures are required to facilitate reproducibility and classification of the measurements, for example, to achieve consistent sample-to-sample and laboratory-to-laboratory results.

Convergent and reproducible values of the heat of immersion can be obtained using pyrogenic silica particles that were subjected to a sequence of thermal treatments, such as by Taylor et al. and Balard et al. (Figure S1a-e).[1,5] Pyrogenic silica consists of non-porous small particles with diameters of 5 to 50 nm, which tend to agglomerate to form larger particles. Thereby, smaller particles in between larger particles create void spaces (called intraparticle pores or cavities) with internal silanol and water content. A specific sequence of steps of thermal treatment and rehydration enables the preparation of uniform Q^3 surfaces with well-defined surface area: (1) heating the samples to 115 ºC evaporates water on the surface of particles (Figure S1a,b), (2) heating to >700 ºC evaporates internal water inside cavities and condensates internal silanol groups in the form of siloxane bridges leading to the collapse of cavities, and condensates a fraction of the surface silanol groups (Figure S1b,c), (3) rehydration and cooling to room temperature reforms superficial silanol groups while internal cavities remain irreversibly

collapsed (Figure S1c,d), (4) subsequent heating to 115 ºC removes adsorbed water molecules from the particle surfaces again, leaving the particles dry and ready for measurements (Figure S1d,e). Measurements of the area density of surface silanol groups indicate 4.7±0.1 per nm^2 for several batches of pyrogenic silica samples. The heat of immersion for these well prepared silica particles was reported as 160±5 mJ/m^2 at 300 K and serves as a reference value for the simulation.[1,5]

Measurements of the enthalpy of immersion were carried out by microcalorimetry in pure water with negligible ionic strength. Under these conditions, surface ionization of silanol groups is very low at <0.05/nm^2 (<1% ionization of SiOH on Q^3 surfaces).[40] Hence, the 0% ionized model of a Q^3 silica surface was chosen in the calculation of the heat of immersion in molecular dynamics simulation (Figure 5a).

Information on the area density of silanol groups, porosity, and initial humidity can be used to build appropriate models for other silica surfaces and nanoparticles to compute hydration energies. For example, quartz surfaces with a higher, Q^2-like area density of silanol groups and silica particles containing nanometer-sized pores and internal cavities exhibit immersion enthalpies up to an order of magnitude higher.

S6. Details on Contact Angles

The experimental measurement of equilibrium contact angles q was performed as an average of advancing and receding contact angles ($q = q_E = (q_A + q_R)/2$) of water on quartz plates outgassed between 200 °C and 1000 ºC by Lamb et al[27] on the basis of the Wolfram and Faust equation[63] and assuming a Wenzel surface-roughness of 1.0. Computed contact angles were obtained from superimposed trajectories of 1000 water molecules during the last 2 ns of 5 ns

molecular dynamics simulation time on silica surfaces as large as ~10×10 nm^2 to suppress interactions between water molecules and their mutual periodic images (see section S9 for details).

S7. Details on Adsorption Isotherms and Molecular Structure of the Interface

S7.1. Adsorption Isotherms and Surface Pressure. Adsorption isotherms provide sensitive information on surface interactions, particularly for surfaces that exhibit different topographies upon cleavage or hydration reactions.[35,64] Gravimetric, volumetric, and chromatographic techniques are commonly employed to monitor the adsorbed amount of a solvent q (in mol/m^2) as a function of the vapor pressure P in the gas phase.[8,38,56,65-67] The measurement normally proceeds from bare surfaces near zero pressure $P \sim 0$ via monolayer coverage at $P = P_M$ towards multilayer coverage up to the saturation pressure $P = P_0$ (~3.17 kPa at 298.15 K for water). Adsorption isotherms of Langmuir type are often assumed to fit the data[68,69] and the pressure up to which the adsorption isotherm follows the shape of a Langmuir isotherm is attributed to the vapor pressure corresponding to a monolayer P_M.[8,38,56,65-67] Knowing an estimate of P_M, typically the monolayer surface pressure, or spreading pressure, π (in J/m^2) is then determined by numerical integration of the adsorbed amount q:

$$\pi = \gamma_S - \gamma_{SW} = RT \int_{P=0}^{P=P_M} q \, d\ln P . \qquad \text{(S1)}$$

S7.2. Langmuir Isotherm and Interface Tensions. The Langmuir adsorption isotherm assumes first order adsorption kinetics of gas molecules without self-interactions on a flat substrate.[69] Under these conditions, the fraction of filled surface sites θ up to formation of a

molecular monolayer (typically <4 Å thick) is related to a material and temperature dependent constant α and the pressure *P:*

$$\theta = \frac{\alpha P}{1 + \alpha P}. \qquad \text{(S2)}$$

Often multilayer formation follows and the pressure corresponding to monolayer adsorption is estimated from the adsorption isotherm to evaluate the surface pressure π (equation S1).[68] The assumption of clean monolayer formation is strictly true for inert gases such as noble gases and N_2 while additional interactions such as hydrogen bonds or chain folding for larger molecules lead to significant molecule-molecule interactions and formation of partial multilayers (>4Å thickness) even before monolayer coverage is reached. An example is the water interface according to the computation that shows multilayer formation even at low surface coverage (Figure S2).

Measurements of water adsorption isotherms on silica were performed by various groups and the variety of possible silica surface structure leads to a spectrum of adsorption isotherms and surface pressures that resembles the variety of immersion energies and contact angles.[8,38,56,65-67] Reproducible isotherms were measured by Baker et al[38] on non-porous pyrogenic silica particles (TK 800-II) outgassed at 25 ºC with a Si-OH density of ~4.1/nm^2, by Muster et al[47] on non-porous colloidal silica particles outgassed at 25 ºC with a Si-OH density of ~4.6/nm^2, and by Zhuravlev[50] on wide-pore silica gel heat treated in vacuo at 200ºC with a Si-OH density of ~4.6/nm^2 (Figure 7). The pore diameter was not specifically reported but it was mentioned that particles feature solely wide pores in order to be eligible for the measurements. The monolayer vapor pressure P_M is attributed to the pressure up to which the adsorption isotherm follows the shape of a Langmuir isotherm, and this pressure is reported in a range of P/P_0 = 0.2 to 0.3 (P_0 ~

3.17 kPa at 298.15 K). Similar results for comparable samples were obtained by other groups as well.[8,38,56] The pressure for adsorption of a half monolayer was reported as P/P_0~0.125.

In addition, a wide range of surface tensions and surface-water interface tensions has been derived from measured surface pressures π according to equation S1.[56] The evaluation of the balance of interfacial energies and of the solid-water interface tension γ_{SW} is challenging using such data from adsorption isotherms, however, because a surface coverage of at least four to six molecular layers of water is needed to form distinguishable solid-water and liquid-vapor interfaces (Figure 8). Otherwise, solid-liquid, solid-vapor, and liquid-vapor interfacial tensions cannot be accurately determined. Such potential ambiguities were avoided by the direct comparison of adsorption isotherms in experiment and simulation, rather than interfacial energies that may be associated with definition problems.

S7.3. Simulation Results and Molecular Interpretation of the Interface. In the simulation, we employed a Q^3 silica surface at 0% ionization, corresponding to deionized water,[40] the Gibbs Ensemble method, freely movable surface atoms, the SPC water model, and extensive equilibration for pressures from 0 kPa to 1 kPa ($P/P_0 =$ 0 to 0.35, see section S9 for details).

Computed and measured adsorption isotherms are in good quantitative agreement (Figure 7). A complete monolayer is formed near P/P_0 = 0.25 and surface pressures π at P/P_0 = 0.25 are obtained as 24, 28, 21, 20 mJ/m^2 for the data by Muster et al,[47] Zhuravlev,[50] Baker et al,[38] and simulation according to equation S1. The computational results are at the lower end of measurements as in the adsorption isotherms, and several factors contribute to this result.

(1) The use of Q^3 surfaces with 4.7 silanol groups per nm^2 leads to slightly higher adsorption compared to 4.1-4.6 silanol groups per nm^2 in the measurements, i.e., slightly widens the gap

between simulation results compared to measurements. (2) The amount of adsorbed water in Figure 7 was determined from water molecules within monolayer distance in the density profile (Figure S2, see section S9 for computational details). The true amount of adsorbed water, taken partial multilayers into account, is up to 50% higher and compensates the entire balance. It is then also imperative to correct the notion of "monolayer coverage" that appears to be inapplicable. (3) A slight underestimate of the adsorbed amount also arises from the static dipole moment in the SPC water model. The dipole moment of water increases about 30% upon adsorption from the gas phase to the liquid state in experiment,[21,70] which increases true adsorption relative to the computed values in Figure 6. The computation of the adsorption isotherm is thus affected by the accurate representation of three interfaces in the model, i.e., silica-vapor, silica-liquid, and liquid-vapor, of which the liquid-vapor interface does not involve parameters for silica. Adsorption isotherms may this not the best measure to evaluate the parameters for silica unless a very accurate water model (that reproduces the liquid-vapor interface) is used.

The formation of multilayers even at low surface coverage is a remarkable result from simulation. The density profile shows that even at low pressure P/P_0 some water adsorbs directly onto the surface and additional water remains bound further away from the surface, up to nearly 1 nm distance (Figure S2). The formation of multilayers is supported by the protrusion of silanol groups from the surface and availability of hydrogen bonds. The attraction of water from the gas phase leads to nucleation of water clusters on the silanol groups and on adsorbed water molecules immediately bound to the surface, different from the ideal Langmuir model of adsorbed inert gas molecules that do not interact with each other on a flat, attractive substrate.

Further details of the surface structure of adsorbed water and the role of silanol groups follow from geometry considerations. The volume of one water molecule is 29.9 $Å^3$ per molecule at 1 g/cm^3 density, which leads to an area requirement of ~10 $Å^2$ in a continuous monolayer of water molecules. Accordingly, full monolayer coverage corresponds to 10 molecules per nm^2 (17 $\mu mol/m^2$). However, the amount of adsorbed water for monolayer coverage is only 3.5 to 4.7 molecules per nm^2 (6-8 $\mu mol/m^2$) (Figure 7). The difference mostly consists of silanol groups that protrude from the surface into the aqueous phase (Figure 1a-c) and form part of the water monolayer at a density of 4.1 to 4.7 per nm^2 (7-8 $\mu mol/m^2$). The sum of both contributions nearly accounts for the total of 10 molecules per nm^2, slightly short due to the rigid positions of silanol groups.

In the computation, we counted only water in the first adsorbed layer towards adsorption and then obtain good agreement with measured adsorption isotherms, about 10-40% short of experimental data (Figure 7). Apart from the neglect of the change in dipole moment upon adsorption, the agreement between experiment and simulation improves if also the second layer of adsorbed water molecules is counted and the total scaled by 90-95% to correct for lower silanol density in experiment (~4.4 instead of ~4.7 per nm^2). The sum of silanol groups (4.3 per nm^2 resp. 7 $\mu mol/m^2$), the first molecular layer of water (2.7 per nm^2 resp. 5 $\mu mol/m^2$), and all additional adsorbed water (3.5 per nm^2 resp. 6 $\mu mol/m^2$) at P/P_0=0.25 amounts to 10.5 per nm^2 (18 $\mu mol/m^2$). This value corresponds to the expectation for genuine monolayer coverage with ~10 water molecules per nm^2, and thus demonstrates near-quantitative consistency between simulation and measurements.

The interpretation at a molecular level also shows that Langmuir-type adsorption isotherms are only approximate, or perhaps not applicable for water on silica. It is also not certain whether

all water in the diffuse multilayers is gravimetrically registered during measurements. Therefore, some ambiguity of comparisons between experiment and simulation may be clarified in further studies. For validation of the force field, the heat of immersion is simpler and unequivocal.

S8. Parallels in Swelling of Silica and Clay Minerals

We find close parallels between silica surfaces and clay minerals, which form layered structures of higher definition and have been systematically studied with regard to hydration.[71,72] Swelling of montmorillonite in water is well known for cation exchange capacities (CEC) in the range 90±30 meq/100g, which corresponds to 0.71±0.24 Na^+ ions per nm^2,[22,73,74] equal to 14±5% ionization of silanol groups on Q^3 silica surfaces (green, light blue, and orange curve in Figure 9). Swelling is also known for clays with CECs up to 140 meq/100g, similar to silica with 22% ionization (close to the red curve in Figure 8). In addition, dissociation of few cations has been reported for mica surfaces with a high cation density of 2.14 K^+ ions per nm^2, equal to 46% ionization of silanol groups on a Q^3 silica surface (black curve in Figure 9). While such high ionization is somewhat hypothetical for silica, the portion of dissociated ions is also small. The similarities show that the cation density per surface area is a key quantity for mineral surfaces with electric double layers and affects properties of aqueous interfaces in comparable ways.

Besides, there are also some differences between silica and clay surfaces: (1) The presence of OH groups renders Q^3 and Q^2 silica surfaces always hydrophilic, even when no ionization takes place. Clay surfaces are Q^4 surfaces and are thus partly hydrophobic in the absence of anionic-cationic defects. Therefore, clay surfaces at very low CEC exhibit no swelling and behave similar to Q^4 silica surfaces. (2) Cations are locally attracted to superficial SiO^- groups on silica while they are attracted to AlO_2^- charge defects in the outer tetrahedral sheet or to $MgO(OH)^-$

defects in the inner octahedral sheet of clay minerals. The negative charge in clay mineral layers is more delocalized across several oxygen atoms and less closely approached by cations than on silica surfaces.[21,71]

Recently, also iron titanates with a very high area density of protons over 3 per nm^2 have been described.[75] A large area density of voluminous positively charged amine bases can then be enforced through an exergonic protonation reaction that results in reversible swelling (gallery expansion) by a factor of one hundred.

S9. Computational and Experimental Details.

S9.1. Models. Models of unit cells of α-cristobalite and α-quartz were obtained from published X-ray crystal structures[2-4] to create super cells of the minerals (Table 5). Models of regular Q^3 and Q^2 surfaces of approximately ~3.5×3.5 nm^2 surface area were obtained by cleavage of the $(10\bar{1})$ plane of α-cristobalite and of the (100) plane of α-quartz, respectively, followed by hydration of dissociated bonds to silanol groups (Figure 1a,e).

Models of structurally random amorphous silica were adopted from the shared library of Materials Studio (Figure 1d).[76] The structure in this database was processed to saturate all valences, followed by energy minimization and molecular dynamics simulation to achieve structural stability. Amorphous silica models can also be built from scratch using the Materials Studio Builder module maintaining stoichiometry and coordination numbers of the atoms. The difference between amorphous and crystalline structures consists in lack of translational symmetry, local deviations from equilibrium bond lengths and angles, possible internal cavities with silanol groups, porosity, and surface roughness in variable extent.

Models representing heat-treated silica with lower density of silanol groups were prepared by mimicking the dehydration reaction, i.e., deletion of a hydrogen atom and a hydroxyl group of adjacent silanol groups and introduction of siloxane bridges Si-O-Si, followed by energy minimization (Figure 1f). This procedure adds Q^4 environments onto Q^3 surfaces (Figure 6), and Q^3 environments onto Q^2 surfaces (Figure 1e).

Models of deprotonated surfaces to represent the influence of pH, ionic strength and cations were obtained by deletion of hydrogen atoms of selected ≡Si–OH groups and addition of sodium counter ions to create sodium siloxide groups [$\equiv SiO^- \cdots Na^+$] (Figure 1). Usually the distribution with largest possible distance between ionic groups is close to the lowest energy, and Energy minimization of several possible structures with the same amount of ionic groups and different distribution was employed to determine the structure of lowest energy. The procedure to introduce ionic groups was also applied to amorphous and porous surfaces, whereby the area density of SiO(H, Na) groups and the degree of ionization of SiOH groups remain important parameters (Figure 1d). Small uncertainties in the distribution of ionic groups on the surface are negligible compared to choosing the correct number of ionic groups per surface area. Energy minimization and molecular dynamics simulation, including brief annealing,[77] were carried out for all newly constructed surfaces to obtain equilibrium coordinates.

Models of the interfaces of silica and water were built by combination of surface slabs and water slabs using the graphical interface of Materials Studio. This input could be directly used for simulations with the PCFF-INTERFACE force field. For use of the CHARMM-INTERFACE and AMBER-INTERFACE force fields, two further steps were required. In the first step, models of the surface slab and the water slab were prepared separately in .pdb and .psf format. In the second step, these slabs were combined into one uniform .pdb/.psf model. Two programs

routines provided in the SI were employed for these tasks. The definition of specific CHARMM topology files appeared less practical due to the bonded nature and structural complexity of silica (quartz, cristobalite, amorphous, porous, etc).

Molecular representations were visualized using the Materials Studio graphical user interface.[76]

S9.2. Cell Parameters. Cell parameters of the unit cell were computed using models of approximately 2.5x2.5x2.5 nm^3 size (Table 5) and NPT molecular dynamics simulation at 298.15 K and atmospheric pressure. The total simulation time was 1 ns (50 ps sufficient to achieve convergence) with a time step of 0.5 fs, a cutoff for van-der-Waals interactions at 1.2 nm, Ewald or PPPM summation of Coulomb interactions with high accuracy of 10^{-6}, pressure control by Parrinello-Rahman method or Nose-Hoover chains, and temperature control by the Andersen thermostat or Nose-Hoover chains. We employed the Discover program of Materials Studio,[76] LAMMPS,[78] and NAMD[79] for the different force field versions (PCFF-INTERFACE, CHARMM-INTERFACE, AMBER-INTERFACE). Computed equilibrium cell parameters are essentially the same using the PCFF, CHARMM, or AMBER version (see Table 5 and comparison of equilibrium densities in Table S1).

S9.3. Vibration Spectrum. The superposition of Infrared and Raman spectra of bulk silica terminated by a Q^3 surface was calculated from the Fourier transform of the velocity autocorrelation function of all atoms (Figure 4). First, a supercell of α-cristobalite of about 2.5x2.5x2.5 nm^3 size was relaxed during 200 ps molecular dynamics simulation in the NVT ensemble at 298.15 K at equilibrium density. MD calculations were continued for 20 ps, recording snapshots every 1 fs. Then, the velocity autocorrelation function of all atoms was computed, followed by the Fourier transform to yield the vibration spectrum. The presence of all

major peaks at similar wavenumbers as in laboratory data is seen (within ±20 cm^{-1}) and peak positions of α-quartz and α-cristobalite are similar (see also further data in ref. [14]). The Materials Studio graphical interface, Discover, and Forcite programs were employed.[76]

S9.4. Heat of Immersion. The hydration energy of a given silica surface was calculated using three distinct simulation boxes containing the silica-water interface, the silica-vacuum interface, and water under periodic boundary conditions (Figure 5). Molecular dynamics simulations were carried out for each of the three systems using Q^3 silica surfaces of about 3.5x3.5 nm^2 cross-sectional area with 0% ionization (as well as with 4% ionization for further tests) and 1600 water molecules. The silica-vacuum system was built by removal of water molecules from the surface-water system and extension of the box height to 30 nm. Equilibrium box dimensions for silica-water and water only systems, as well as the equilibrium dimension of the silica slab in the *xy* plane were initially obtained by NPT simulation under standard conditions. Each system was then subjected to MD simulation of five ns duration using the NVT ensemble at 300 K, corresponding to conditions of laboratory measurements.[1,5] Average energies over the last 4 ns of each trajectory were used to compute the heat of hydration as a difference in total energy between the three systems, normalized by the silica-water interfacial area 2*A* (Figure 5a). The interfacial area corresponds to two times the cross-sectional area due to periodic boundary conditions. The simulations were performed using a time step of 1 fs, a cutoff of 1.2 nm for van-der-Waals interactions, and summation of Coulomb interactions with the PPPM method with high accuracy of 10^{-6} using the LAMMPS program.[78] Statistical uncertainties were estimated from block averages of the energy over major fractions of the total simulation time. TIP3P, flexible SPC, and PCFF water models lead to the same heat of immersion within ±5 mJ/m^2.

S9.5. Contact Angle. Contact angles were computed using MD simulation of 1000 water molecules in the NVT ensemble at 298.15 K on different silica surfaces with 0% ionization. Four different surfaces covering a range of pure Q^3 to pure Q^4 environments were employed. The water molecules were initially placed in a cylindrical configuration. The dimensions of the surfaces were ~10×10 nm^2 to allow spreading of water molecules and avoid interactions with periodic images (Figure 6). The total simulation time was 3 ns, of which the first 1 ns served for equilibration and the last 2 ns were used to collect data. The obtained trajectories of superficial water were visualized using the VMD graphical interface[80] and superimposed to obtain a statistically averaged geometry of the water droplets formed. Contact angles were then graphically analyzed from rendered images, including measurements at various rotation angles (steps of 15°) in the *xy* plane. Average values are reported and the statistical uncertainty was less than ±3°. The flexible SPC water model was employed, and the program LAMMPS for simulations.[78]

S9.6. Adsorption Isotherm. The adsorption isotherm of water vapor onto a regular Q^3 silica surface with 0% ionization was studied using Gibbs Ensemble Monte Carlo simulation[81] with the Towhee program (Figure 7).[19] The cross-sectional area of the surface was approximately 3.5x3.5 nm^2, and 500 water molecules (SPC model) were employed. The adsorbed amount of water was obtained under NPT conditions at 298.15 K for pressures starting near zero up to ~1 kPa, equivalent to P/P_0 ranging from 0 to 0.35 (P_0~3.17 kPa at 298.15 K). For each pressure setting, 140000 Monte Carlo cycles were performed in total, of which each cycle involved 500 independent Monte Carlo moves, i.e., $7 \cdot 10^7$ moves total. 60000 cycles served for equilibration and 80000 cycles for data recording. Surface atoms were fixed during equilibration and flexible during data recording. Initially, all water molecules were positioned in the gas phase. Monte

Carlo moves included translation of the center of mass of water molecules and rotation around the center of mass of water molecules, exchange moves between the two simulation boxes, volume changes of the simulation box representing the vapor phase, as well as translation moves of single atoms on the silica surface (during data recording). The weighting of the types of possible moves was adjusted such that the acceptance ratio exceeded 50%. Density profiles of water molecules adsorbed onto the silica surface were used to identify the height of a monolayer (Figure S2). The time-average number count of water molecules in the first layer was used to quantify the adsorbed amount and to plot the computed adsorption isotherms (Figure 7). Statistical uncertainties in the adsorbed amount were obtained from differences in block averages during major portions of the data recording phase of the simulation.

S9.7. Density Profiles and Sodium Dissociation. Density profiles of aqueous silica interfaces were computed using regular Q^3 surfaces of approximately 3.5x3.5 nm^2 cross-sectional area and 2.5 nm thickness in contact with 1600 water molecules in NPT molecular dynamics simulation under standard conditions (Figures 8 and 9). The simulation time was 21 ns, and the position of water oxygen atoms as well as sodium ions was recorded every 10 ps using small bins of 0.01 Å size along the *z* direction (Figures 8, 9, 10). Data are shown as an average over all water molecules and all sodium ions over the last 20 ns simulation time. Numerical uncertainties are negligible due to the large number of data points.

Supporting References

(1) Taylor, J. A. G.; Hockey, J. A. *J. Phys. Chem.* **1966**, *70*, 2169.

(2) Kihara, K. *Eur. J. Mineral.* **1990**, *2*, 63.

(3) *Silica: Physical Behavior, Geochemistry, and Materials Applications*; Heaney, P. J., Prewitt, C. T., Gibbs, G. V., eds., In: Reviews in Mineralogy, Vol. 29; Mineralogical Society of America: New Jersey, USA, 1994.

(4) Dera, P.; Lazarz, J. D.; Prakapenka, V. B.; Barkley, M.; Downs, R. T. *Phys. Chem. Miner.* **2011**, *38*, 517.

(5) Balard, H.; Donnet, J.-B.; Oulanti, H.; Gottschalk-Gaudig, T.; Barthel, H. *Colloids Surf., A* **2011**, *378*, 38.

(6) Kondo, S.; Fujiwara, H.; Ichii, T.; Tsuboi, I. *J. Chem. Soc., Faraday Trans. I* **1979**, *75*, 646.

(7) Donnet, J.-B. B., H.; Nedjari, N.; Hamdi, B.; Barthel, H.; Gottschalk-Gaudig, T. *J. Colloid Interface Sci.* **2008**, *328*, 15.

(8) Douillard, J. M.; Elwafir, M.; Partyka, S. *J. Colloid Interface Sci.* **1994**, *164*, 238.

(9) Legrand, A. P. *The Surface Properties of Silica*; John Wiley & Sons: New York, 1998, p. 72.

(10) Partyka, S.; Rouquerol, F.; Rouquerol, J. *J. Colloid Interface Sci.* **1979**, *68*, 21.

(11) Howard, F. L.; Culbertson, J. L. *J. Am. Chem. Soc.* **1950**, *72*, 1185.

(12) Sanders, M. J.; Leslie, M.; Catlow, C. R. A. *J. Chem. Soc., Chem. Commun.* **1984**, 1271.

(13) Feuston, B. P.; Garofalini, S. H. *J. Chem. Phys.* **1988**, *89*, 5818.

(14) Garofalini, S. H. *J. Chem. Phys.* **1982**, *76*, 3189.

(15) van Beest, B. W. H.; Kramer, G. J. *Phys. Rev. Lett.* **1990**, *64*, 1955.

(16) Hill, J. R.; Sauer, J. *J. Phys. Chem.* **1994**, *98*, 1238.

(17) Hill, J. R.; Sauer, J. *J. Phys. Chem.* **1995**, *99*, 9536.

(18) Maple, J. R.; Thacher, T. S.; Dinur, U.; Hagler, A. T. *Chem. Des. Autom. News* **1990**, *5*, 5.

(19) Sun, H. *J. Comput. Chem.* **1994**, *15*, 752.

(20) Sun, H. *Macromolecules* **1995**, *28*, 701.

(21) Heinz, H.; Suter, U. W. *J. Phys. Chem. B* **2004**, *108*, 18341.

(22) Heinz, H.; Koerner, H.; Anderson, K. L.; Vaia, R. A.; Farmer, B. L. *Chem. Mater.* **2005**, *17*, 5658.

(23) Heinz, H.; Vaia, R. A.; Farmer, B. L.; Naik, R. R. *J. Phys. Chem. C* **2008**, *112*, 17281.

(24) Heinz, H.; Lin, T. J.; Mishra, R. K.; Emami, F. S. *Langmuir* **2013**, *29*, 1754.

(25) Patwardhan, S. V.; Emami, F. S.; Berry, R. J.; Jones, S. E.; Naik, R. R.; Deschaume, O.; Heinz, H.; Perry, C. C. *J. Am. Chem. Soc.* **2012**, *134*, 6244.

(26) Cruz-Chu, E. R.; Aksimentiev, A.; Schulten, K. *J. Phys. Chem. B* **2006**, *110*, 21497.

(27) Lamb, R. N.; Furlong, D. N. *J. Chem. Soc., Faraday Trans. 1 F* **1982**, *78*, 61.

(28) Hassanali, A. A.; Singer, S. J. *J. Phys. Chem. B* **2007**, *111*, 11181.

(29) Hassanali, A. A.; Zhang, H.; Knight, C.; Shin, Y. K.; Singer, S. J. *J. Chem. Theory Comput.* **2010**, *6*, 3456.

(30) Lopes, P. E. M.; Murashov, V.; Tazi, M.; Demchuk, E.; MacKerell, A. D. *J. Phys. Chem. B* **2006**, *110*, 2782.

(31) Lockwood, G. K.; Garofalini, S. H. *J. Chem. Phys.* **2009**, *131*, 074703.

(32) Butenuth, A.; Moras, G.; Schneider, J.; Koleini, M.; Köppen, S.; Meißner, R.; Wright, L. B.; Walsh, T. R.; Ciacchi, L. C. *Phys. Status Solidi B* **2012**, *249*, 292.

(33) Chenoweth, K.; van Duin, A. C. T.; Goddard III, W. A. *J. Phys. Chem. A.* **2008**, *112*, 1040.

(34) Heinz, H.; Vaia, R. A.; Farmer, B. L. *J. Chem. Phys.* **2006**, *124*, 224713.

(35) Mishra, R. K.; Flatt, R. J.; Heinz, H. *J. Phys. Chem. C* **2013**, *117*, 10417.

(36) Tadros, T. F.; Lyklema, J. *J. Electroanal. Chem. Interfacial Electrochem.* **1968**, *17*, 267.

(37) Handke, M.; Mozgawa, W. *Vib. Spectrosc.* **1993**, *5*, 75.

(38) Baker, F. S.; Sing, K. S. W. *J. Colloid Interface Sci.* **1976**, *55*, 605.

(39) Bolt, G. H. *J. Phys. Chem.* **1957**, *61*, 1166.

(40) Abendroth, R. P. *J. Colloid Interface Sci.* **1970**, *34*, 591.

(41) Yates, D. E.; Healy, T. W. *J. Colloid Interface Sci.* **1976**, *55*, 9.

(42) Milonjić, S. K. *Colloids Surf.* **1987**, *23*, 301.

(43) Zerrouk, R.; Foissy, A.; Mercier, R.; Chevallier, Y.; Morawski, J.-C. *J. Colloid Interface Sci.* **1990**, *139*, 20.

(44) House, W. A.; Orr, D. R. *J. Chem. Soc., Faraday Trans.* **1992**, *88*, 233.

(45) Sonnefeld, J. *J. Colloid Interface Sci.* **1996**, *183*, 597.

(46) Méndez, A.; Bosch, E.; Rosés, M.; Neue, U. D. *J. Chromatogr. A* **2003**, *986*, 33.

(47) Muster, T. H.; Prestidge, C. A.; Hayes, R. A. *Colloids Surf., A* **2001**, *176*, 253.

(48) Zhuravlev, L. T. *Langmuir* **1987**, *3*, 316.

(49) Zhuravlev, L. T. *Colloids Surf., A* **2000**, *173*, 1.

(50) Zhuravlev, L. T. *Colloids Surf., A* **1993**, *74*, 71.

(51) Emami, F. S.; Puddu, V.; Berry, R. J.; Varshney, V.; Patwardhan, S. V.; Perry, C. C.; Heinz, H. *Submitted*.

(52) Heinz, H.; Castelijns, H. J.; Suter, U. W. *J. Am. Chem. Soc.* **2003**, *125*, 9500.

(53) *CRC Handbook of Chemistry and Physics* 89th, Lide, D. R., ed.; CRC Press: Boca Raton, FL, 2008.

(54) Batsanov, S. S. *Inorg. Mater.* **2001**, *37*, 871.

(55) Halgren, T. A. *J. Am. Chem. Soc.* **1992**, *114*, 7827.

(56) Helmy, A. K.; de Bussetti, S. G.; Ferreiro, E. A. *Appl. Surf. Sci.* **2007**, *253*, 6878.

(57) Zartman, G. D.; Liu, H.; Akdim, B.; Pachter, R.; Heinz, H. *J. Phys. Chem. C* **2010**, *114*, 1763.

(58) Heinz, H. *J. Comput. Chem.* **2010**, *31*, 1564.

(59) Levien, L.; Prewitt, C. T.; Weidner, D. J. *Am. Mineral.* **1980**, *65*, 920.

(60) Oliver, W. C.; Pharr, G. M. *J. Mater. Res.* **1992**, *7*, 1564.

(61) Fubini, B. *Thermochim. Acta* **1988**, *135*, 19.

(62) Kiselev, A. V. *Surface Chemical Compounds and Their Role in Adsorption Phenomena*; Moscow University Press: Moscow, 1957.

(63) Wolfram, E.; Faust, R. In *Wetting, Spreading, and Adhesion*; Padday, J. F., Ed.; Academic Press: London, 1978, p 213.

(64) Jacobs, J. D.; Koerner, H.; Heinz, H.; Farmer, B. L.; Mirau, P. A.; Garrett, P. H.; Vaia, R. A. *J. Phys. Chem. B* **2006**, *110*, 20143.

(65) Boyd, G. E.; Livingston, H. K. *J. Am. Chem. Soc.* **1942**, *64*, 2383.

(66) Hackerman, N.; Hall, A. C. *J. Phys. Chem.* **1958**, *62*, 1212.

(67) Staszczuk, P. *Chromatographia* **1985**, *20*, 724.

(68) Brunauer, S.; Emmett, P. H.; Teller, E. *J. Am. Chem. Soc.* **1938**, *60*, 309.

(69) Langmuir, I. *J. Am. Ceram. Soc.* **1918**, *40*, 1361.

(70) Mahoney, M. W.; Jorgensen, W. L. *J. Chem. Phys.* **2000**, *112*, 8910.

(71) Heinz, H. *Clay Miner.* **2012**, *47*, 205.

(72) Schoonheydt, R. A.; Johnston, C. T. In *The Surface Properties of Clay Minerals*; Brigatti, M. F., Mottana, A., Eds.; The European Mineralogical Union: 2011.

(73) Fu, Y.-T.; Heinz, H. *Chem. Mater.* **2010**, *22*, 1595.

(74) Heinz, H.; Vaia, R. A.; Krishnamoorti, R.; Farmer, B. L. *Chem. Mater.* **2007**, *19*, 59.

(75) Geng, F.; Ma, R.; Nakamura, A.; Akatsuka, K.; Ebina, Y.; Yamauchi, Y.; Miyamoto, N.; Tateyama, Y.; Sasaki, T. *Nature Comm.* **2013**, *4*, 1632.

(76) Accelrys Inc: San Diego, CA, 2006.

(77) Fu, Y. T.; Heinz, H. *Chem. Mater.* **2010**, *22*, 1595.

(78) Plimpton, S. *J. Comput. Phys.* **1995**, *117*, 1.

(79) Phillips, J. C.; Braun, R.; Wang, W.; Gumbart, J.; Tajkhorshid, E.; Villa, E.; Chipot, C.; Skeel, R. D.; Kale, L.; Schulten, K. *J. Comput. Chem.* **2005**, *26*, 1781.

(80) Humphrey, W.; Dalke, A.; Schulten, K. *J. Mol. Graphics* **1996**, *14*, 33.

(81) Panagiotopoulos, A. Z.; Quirke, N.; Stapleton, M.; Tildeseley, D. J. *Mol. Phys.* **1988**, *63*, 527.